Engineering Failure Analysis 154 (2023) 107690

Contents lists available at ScienceDirect

Engineering Failure Analysis

journal homepage: www.elsevier.com/locate/engfailanal

Fatigue life simulation of AA7075-T651 FSW joints using experimental data

Jafar Langari [a,*], Karim Aliakbari [b,*], Farhad Kolahan [c]

[a] Department of Mechanical Engineering, Faculty of Engineering, University of Bojnord, Bojnord, Iran
[b] Department of Mechanical Engineering, Technical and Vocational University (TVU), Tehran, Iran
[c] Mechanical Engineering Department, Faculty of Engineering, Ferdowsi University of Mashhad, Mashhad, Iran

ARTICLE INFO

Keywords:
Friction stir welding (FSW)
AA7075-T651
Welding parameters
Finite element analysis (FEA)
Mechanical properties
Fatigue behavior

ABSTRACT

The friction stir welding (FSW) process is a solid phase type applied in this study to connect AA7075-T651 aluminum alloy plates. This study investigates the impact of welding input quantities such as tool rotational speed, welding speed, shoulder radius, and tool geometry on welding joint quality, including strength, toughness, hardness, fractography, and fatigue behavior. Also, in this study, the fatigue life in the base material (BM) and joints obtained from the simple, threaded, and truncated triangular pyramid pins as an FSW effective input parameter was obtained by the finite element analysis (FEA). The experimental outcomes represented that the mechanical attributes of the threaded pin are higher than that of the simple and truncated triangular pyramid pins with the same input parameters. Also, the outcomes of the numerical simulation with the experimental outcomes of fatigue life for the BM were in acceptable agreement, and the error value of the validation result for $\sigma_{max} = 0.5\sigma_y$ for the stress ratio $R = -1$ was equal to 0.4%. In addition, the FEA results indicated that the fatigue strength of FSW joints in the stir zone for the threaded, simple, and truncated triangular pyramid pins in the fatigue life of 10^7 cycles was 64%, 63%, and 43% of the BM, respectively.

1. Introduction

Friction stir welding (FSW) is one of the newest procedure of solid phase welding, which has many advantages for aluminum and composite alloys compared to conventional fusion welding methods, due to the low input temperature and lack of melting and refreezing of materials [1,2].

The first focus of the literature review was the mechanical properties and microstructure under different input quantities such as tool rotational speed, welding speed, tool geometry, and type of alloy welded by FSW. The FSW process is a complex process in terms of temperature distribution and material flow. Therefore, knowing the behavior of the material at the joint with regard to the welding input quantities and tool geometry is of particular importance [3,4]. Zhang et al. [5] investigated the impact of welding input quantities on the microstructure and mechanical properties of specimens manufactured of super high strength aluminum alloy by FSW with high tool rotational speed and high welding speeds. It was considered that by raising the welding speed or lowering the tool rotational speed of the tool, the grain size of the nugget zones decreases. Moreira et al. [6] examined the mechanical and metallurgical properties of welded butt joints of aluminum alloy 6061-T6 with 6082-T6 by FSW. This study shows that the dissimilar joint welded by

* Corresponding authors.
E-mail addresses: j.langari@ub.ac.ir (J. Langari), karim-aliakbari@tvu.ac.ir (K. Aliakbari).

https://doi.org/10.1016/j.engfailanal.2023.107690
Received 25 July 2023; Received in revised form 15 September 2023; Accepted 1 October 2023
Available online 3 October 2023

Nomenclature

n	Safety factor (-)
R	stress ratio (-)
S_e	Fatigue limit (MPa)
S_y	Yield strength (MPa)
σ_a	Amplitude stress (MPa)
σ_m	Midrange stress (MPa)
σ_{max}	Maximum stress (MPa)
σ_{min}	Minimum stress (MPa)

Subscripts and superscripts

AA	Aluminum alloy
BM	Base material
FEM	Finite element method
FSW	Friction stir welding
HAZ	heat affected zone
HV	Vickers hardness
OM	Optical microscopy
SEM	Scanning electron microscopy
SZ	Stir zone
TMAZ	Thermo-mechanically affected zone
UTS	Ultimate tensile strength
XRF	X-ray fluorescence spectroscopy

the FSW method has intermediate mechanical properties compared to any BM. Silva et al. [7] investigated the impact of joining input quantities on the mechanical properties, microstructural characteristics, and material flow of dissimilar aluminum alloys (3 mm- thick AA2024-T3 AA7075-T6 sheets) manufactured by FSW. Tan et al. [8] tested the tensile and bending strength in the joint of 5A02 aluminum alloy and pure copper by FSW. When the traverse speed parameter was significantly reduced, a defect-free joint was obtained. This in turn caused excellent metallurgical bonding between Al and Cu and resulted in improved tensile and bending strength behavior. Fuller et al. [9] studied the evolution of microstructural and mechanical properties of 7050-T7651 and 7075-T651 Al alloys by FSW as a function of room temperature (natural) aging. During the span of aging times studied, the transverse tensile strength increased continuously, which logical increase for microstructural changes in the light of mechanical properties that can be discussed in the future. Krasnowski et al. [10] studied the impact of tool shape on the microstructure and mechanical properties of Al 6082 alloy joints by the FSW method. Three kinds of tools with various probe shapes and shoulder surfaces and two welding configurations (one-sided and two-sided) were applied in the experiments. The best tensile performance was attained for FSW joints produced by conventional and Triflute tooling. Rodrigues et al. [11] analyzed and compared the friction stir welds produced in 1 mm thin plates of aluminum alloy AA 6016-T4, with two different tools, in terms of microstructure and mechanical properties.

The second focus of the literature review was more emphasis on fatigue behavior in the FSW process. Lukács et al. [12] investigated the behavior of friction stir welded joints under cyclic loading conditions and determined fatigue design curves for two aluminum alloys and their welded joints by the FSW process. The results of high cycle fatigue and fatigue crack growth experiments indicated good correspondence with the results of the comparative base materials. Maddox [13] conducted an overview of methods and relevant codes and standards for the fatigue evaluation of welded aluminum alloy structures. In this research, the assessment methods of aluminum structures have been evaluated from the point of view of initial design and estimation of the residual life of existing structures. Sharma et al. [14] presented the impact of AA7039 BM temperature situations (O, W, and T6) on the fatigue behavior of friction stir welded joints of Al–Zn–Mg alloy AA7039. Their studies showed that FSW of Al–Zn–Mg alloy AA7039 is recommended to be done under W temperature conditions due to better tensile properties and superior fatigue strength. Sillapasa et al. [15] investigated the tensile and fatigue behavior of SZ, HAZ and BM in the FSW joint of rolled 6N01 aluminum alloy plate. Their results showed the bottommost hardness in the HAZ and the highest tensile and fatigue strength in the SZ, which was mainly due to fine and homogeneous grains and significant cyclic hardening. Fatigue failure of the large sheet sample consisting of the entire FSW joint happened at the bottommost hardness location in the HAZ. Liu et al. [16] examined the fatigue characteristics of the A7N01 aluminum alloy welded joint and proposed a model based on fatigue crack initiation life. The total fatigue life estimated using the presented model with the experimental data is in good agreement with the model proposed by Basquin. The observation results of the fractography, using the SEM, showed that the fatigue crack initiates from the smooth surface due to the welding process of the weld metal, and the blowhole in the HAZ causes the fatigue crack to initiate. Cavaliere et al. [17] investigated FSW AA6082 joints using thermoelastic stress analysis to study the crack propagation specifications of friction stir welded aluminum plates. They compared the results obtained by the FEA with the results obtained from the classical CCD camera monitoring of crack front propagation during cyclic loading and these outcomes were in good agreement. Wang et al. [18] examined the very long fatigue and near-threshold fatigue crack growth behavior of 7075 and 6061 Al alloys under T6 conditions. Their results showed that significant surface voids were observed in the two Al-alloys during

Table 1
The chemical composition of AA7075-T651 and standard material (wt %).

Symbol	Mn	Si	Ti	Fe	Cr	Cu	Mg	Zn
AA7075-T651	0.03	0.04	0.075	0.14	0.18	1.4	2.5	5.8
Standard [21]	≤ 0.3	≤ 0.4	≤ 0.2	≤ 0.5	0.18–0.28	1.2–2	2.1–2.9	5.1–6.1

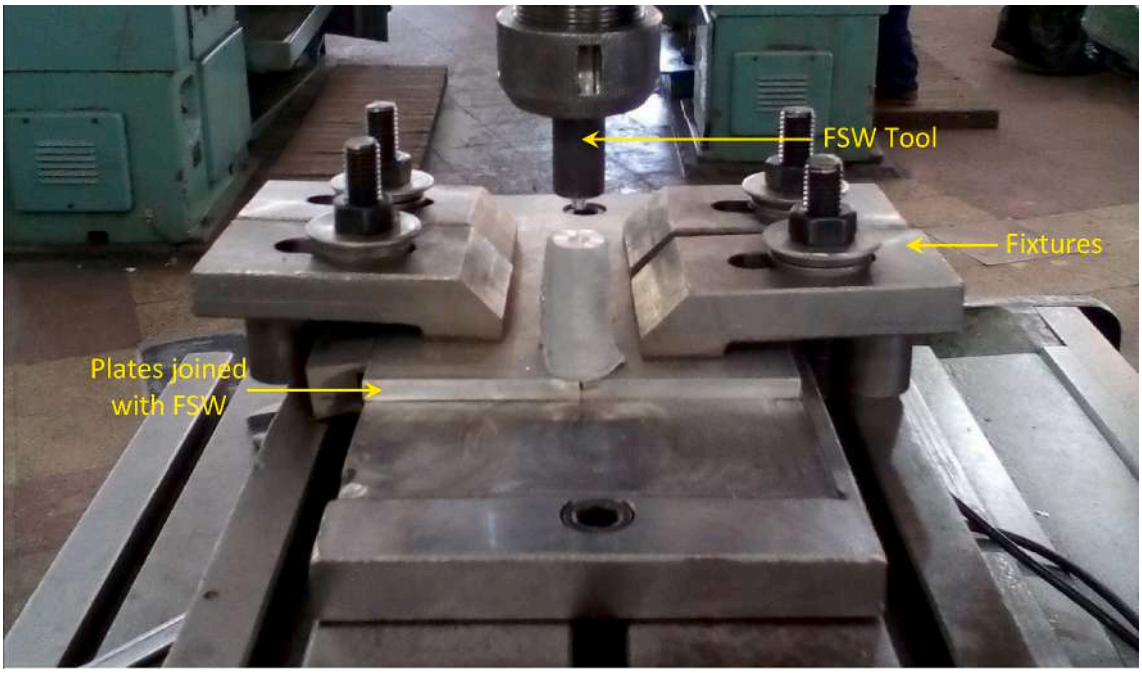

Fig. 1. Complete setup of FSW method.

the crack initiation and early fatigue crack growth process. Furthermore, the fatigue crack growth rate in small cracks in these alloys was greater than in large cracks for the same stress intensity factor range. He et al. [19] presented the results of an experimental examination of the fatigue behavior of FSW joints in AA7075-T6 with an ultrasonic fatigue testing system. Plastic deformation and recrystallization during the welding process led to changes in particle size and the occurrence of microcracks between the TMAZ and the SZ. Therefore, fatigue crack initiation locations tended to be located in the TMAZ during a short fatigue life, or in the SZ in a very high cycle fatigue regime.

Previous studies have mainly focused on the microstructure and mechanical properties of aluminum alloys and dissimilar alloy joints. However, limited literature has focused on fatigue life simulation of FEA in high-strength AA7075-T6 alloy. In particular, the relationship between numerical method results and fatigue life experimental results is not well established. Therefore, the purpose of the present study is to focus on fatigue life simulation using the FEA. Also, in this study, the effect of the simple, threaded, and truncated triangular pyramid pins as effective input parameters on the fatigue life of the BM and welding joints is investigated by the FEA. In addition, the impact of welding input quantities such as tool rotational speed, welding speed, shoulder radius, and tool geometry on welding quality including strength, toughness, hardness, and fractography have also been investigated.

2. Experiments

The sheets used for friction stir welding were rolled aluminum alloy AA7075-T651 with a thickness of 6.35 mm. Table 1 shows the chemical composition of AA7075-T651 rolled aluminum alloy sheets of Russia's Kamensk Uralsky company, which was performed according to ASTM E1251-17a standards [20] by XRF method.

The parameters used for the FSW include the dimensions of the workpiece 6.35 × 120 × 130 mm; tool rotational speed in three levels: 630, 1000, and 1250 rpm; welding speed in three levels of 20, 40, and 60 mm/min; The radius of the shoulder of the tool in two levels is 9 and 11 mm; the upper radius of the tool pin is 8 mm; the bottom radius of the tool pin is 6 mm; the height of the tool pin is 6 mm, and the geometry of the pin is in three levels: simple, threaded, and truncated triangular pyramid. Fig. 1 shows the complete test setup including the FSW machine, tool, workpiece, and fixture.

Fig. 2 shows the full geometric dimensions of the tool as well as the geometry of the pin in three levels: simple, threaded, and truncated triangular pyramid.

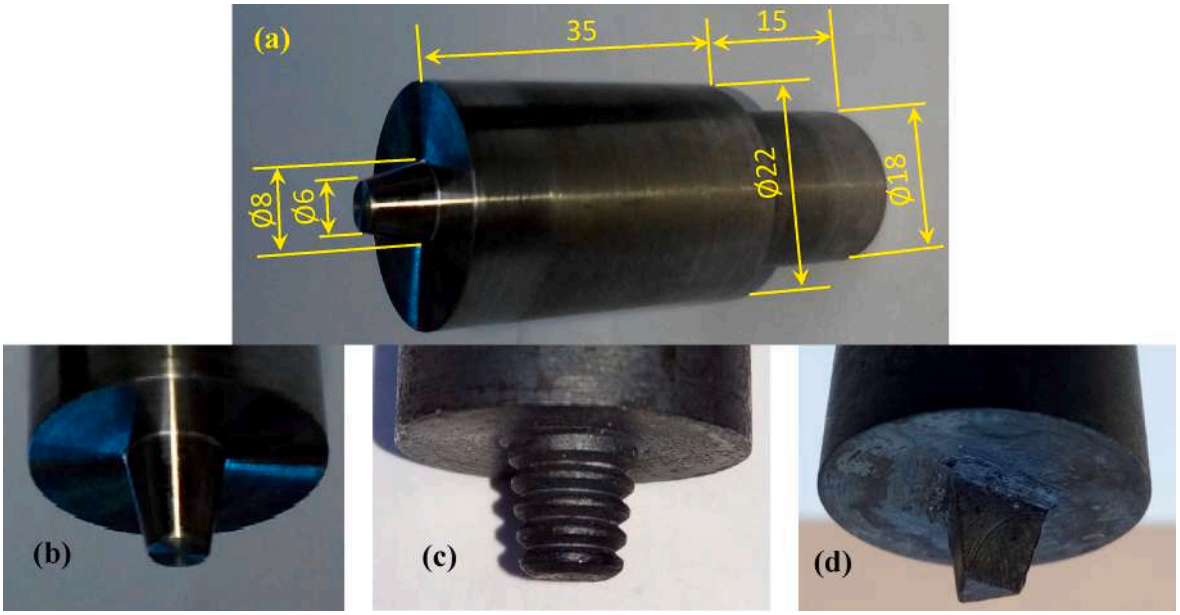

Fig. 2. Tools dimension and geometry of the tool pins; **(a)** Tools dimension, **(b)** Simple, **(c)** Threaded, and **(d)** Truncated triangular pyramid.

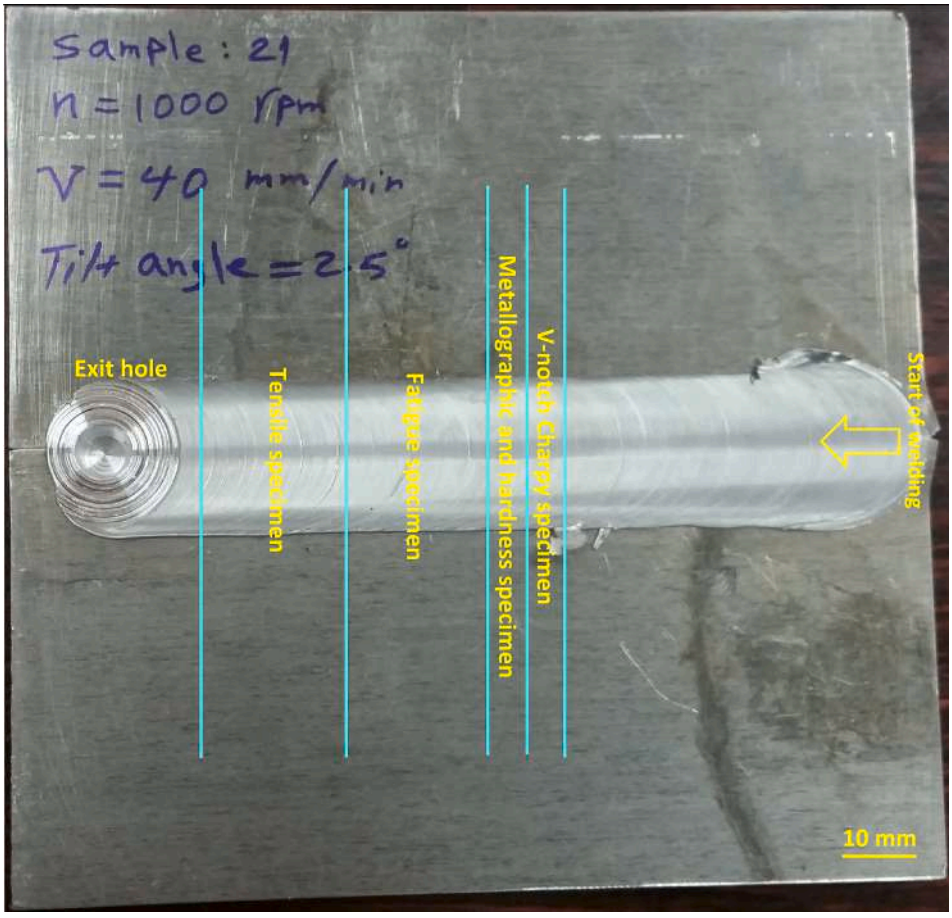

Fig. 3. Extracting the standard samples from the joints.

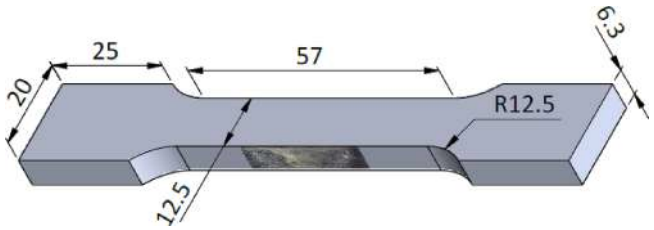

Fig. 4. Specimens geometric dimensions of tensile test used for FSW welding joints and BM (in mm).

Table 2
The mechanical properties of AA7075-T651 and standard material.

Symbol	Ultimate strength (MPa)	Yield strength (MPa)	Modulus of elasticity (GPa)	Poisson's ratio (-)	Elongation (%)	Hardness (HV)
AA7075-T651	570	527	71.7	0.33	12.5	170
Standard [25]	573	516	–	–	–	–

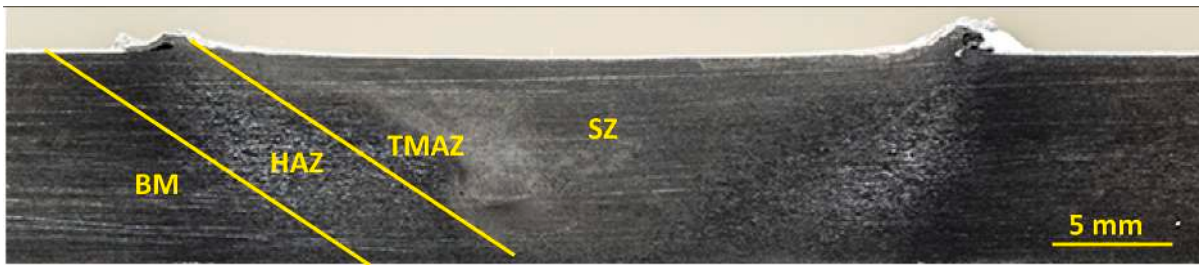

Fig. 5. Cross-sectional macrograph of different welding zones in joints.

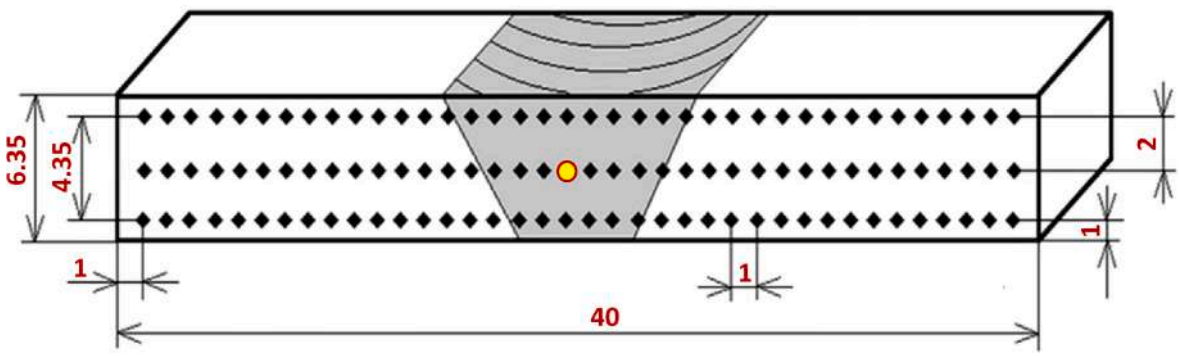

Fig. 6. Cross-sectional macrograph of different welding zones in joints (dimensions in mm).

After welding, the test samples are extracted according to Fig. 3 for experiments. For the tensile sample, three samples were extracted and subjected to tension, and the average results were listed in the table of mechanical properties. For the fatigue sample, a large number of samples were extracted and subjected to the fatigue test and the results were drawn in the graph. For metallography and hardness testing, one sample was extracted from the welding site and the hardness test was obtained in three close rows. But in the present manuscript, the middle hardness measurement results are drawn in the diagram. For the impact sample, three samples have been extracted and subjected to the impact test, and the average results are listed in in the table of the impact energy results.

According to Fig. 4, the tensile test samples of each sheet welded by the FSW method and the BM were prepared to measure the mechanical properties by wire-cut machine. Tensile specimens of sheet type were made from FSW welding joints according to ASTM E8 / E8M-16ae1 standard [22] and Refs [23,24]. Tensile tests were performed using a servo-hydraulic machine under ambient temperature. The outcomes of the tensile test were saved in the form of force–displacement with a sampling rate of 2 times per second. To do the test, the clamps movement speed of the machine was set to 0.50 mm/min. The results of the mechanical properties of the BM and the standard material are listed in Table 2.

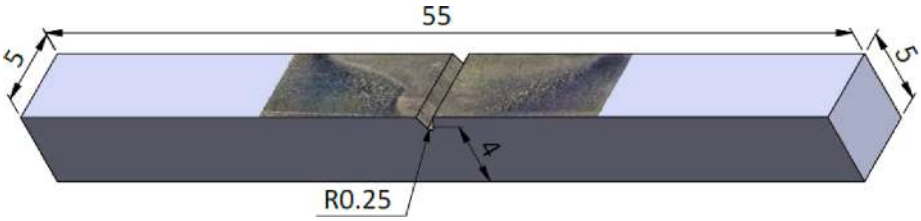

Fig. 7. Specimens geometric dimensions of V-notch Charpy (in mm).

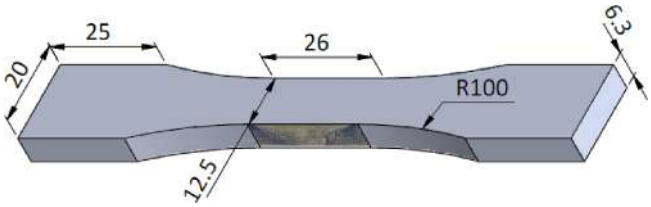

Fig. 8. Dimensions of fatigue samples modeled in CAD software (in mm).

For metallography and hardness testing, extracted samples were sanded and polished. First, for metallography, the surface of the samples was polished with water and Al_2O_3 solution and then etched with 2% Nital solution. Washing with alcohol and drying with hot air were utilized as the final polishing in which Fig. 5 appeared for cross-sectional welding joints. Then as shown in Fig. 6, the hardness test was performed in three close rows according to the ASTM standard: E384-11e1 [26] with a hardness measurement device by applying 200 gr of force for 10 s.

In order to investigate the fractography, SEM images were prepared from the cross-section of the tensile and toughness test samples after the fracture. For this purpose, firstly, the samples were cut from the broken section by EDM wire-cut machine, and the sample was put in an ultrasonic bath for one hour. Then, photos with different magnifications were taken by SEM LEO 1450VP made in Germany.

To specify the Charpy toughness, first, the standard Charpy samples were cut from the FSW welding joint by a wire-cut machine, and the tests were performed at a temperature of 23 °C and a humidity of 20%. At least three specimens were tested for each FSW weld joint and BM as presented in Fig. 7 to achieve the V-notch Charpy energy.

3. Theory and numerical analysis

3.1. Theory

Due to the nature of some rotating machines, fluctuating stresses in industrial equipment are often in the form of a sinusoidal pattern. Therefore, the maximum stress σ_{max} and the minimum stress σ_{min} corresponding to it in a loading cycle can be used to determine the force pattern. For fatigue analysis according to the characteristics of welding joints, the Soderberg failure criterion is used as follows [27].

$$\frac{\sigma_a}{S_e}+\frac{\sigma_m}{S_y}=\frac{1}{n} \tag{1}$$

$$\sigma_a=\left|\frac{\sigma_{max}-\sigma_{min}}{2}\right| \tag{2}$$

$$\sigma_m=\frac{\sigma_{max}+\sigma_{min}}{2} \tag{3}$$

$$R=\frac{\sigma_{min}}{\sigma_{max}} \tag{4}$$

In the above relationships, σ_a, σ_m, S_e, S_y, n, and R are the amplitude stress, midrange stress, fatigue limit, yield strength, safety factor, and stress ratio, respectively.

3.2. 3D finite element analysis

In order to peruse the impact of the weld appearance on the stress concentration in the welding zone, first, a fatigue sample according to Fig. 8 with the details of the weld cross-section was modeled using CAD software according to the ASTM-E466 [28] standard. For the numerical analysis of fatigue, commercial software ANSYS-workbench V18.2 with SOLID 185 element (3D element

Table 3
Outcomes from FE modeling for various elements' number.

Elements	Nodes	Stress (MPa)	Percentage Change
13,032	16,820	189.01	NA
13,717	17,722	184.02	−2.64%
20,840	25,978	183.97	−0.03%
49,818	57,603	184.71	0.02%
129,807	142,360	184.71	0.00%

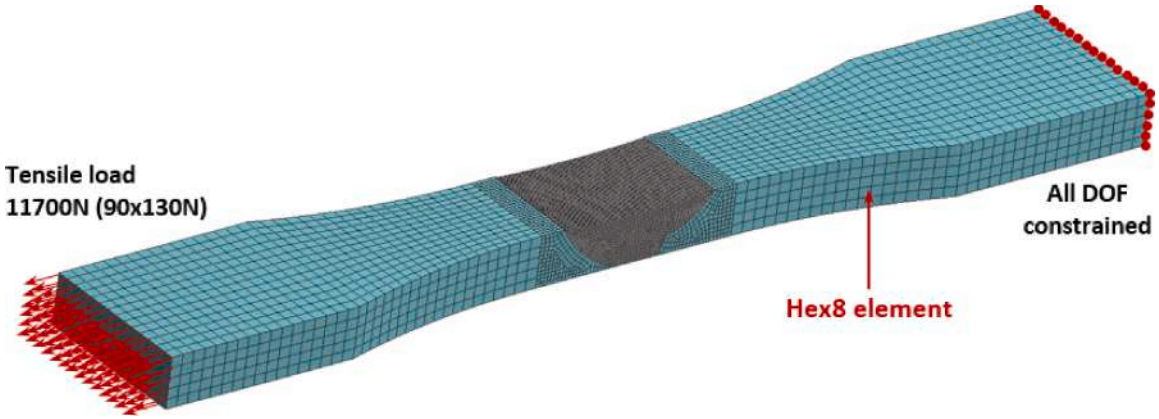

Fig. 9. Meshing, loading, and boundary condition for 3D FE analysis.

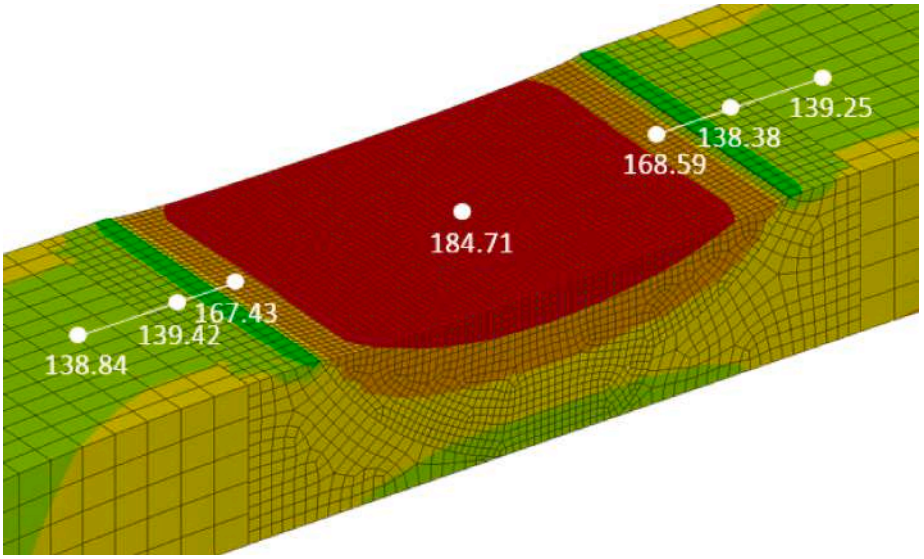

Fig. 10. Stress contour from the result of 3D FE analysis.

with 8 nodes Hex8) was used. The mechanical properties of the weld cross-section and the BM were used from the experimental data of the BM and the joints welded by the FSW [29].

Table 3 demonstrates the solution to the problem in terms of the elements number, the number of nodes, and the stress field in the weld zone for the threaded tool pin. As can be observed, the most suitable number of elements for the SZ is 49,818 and the maximum stress generated in the SZ is 184.71 MPa.

Applied load, boundary conditions, and meshing as shown in Fig. 9 are defined according to Refs [30–32]. Also, Fig. 9 shows the load related to the nominal stress of about 148 MPa, which is one of the nominal stresses with a value of $\sigma_{max} = 0.5\sigma_{yweld}$ of the threaded tool programmed in the static simulation. For this purpose, a load of 130 N is applied to each of the 90 nodes (a total of 11,700 N) located at one end of the fatigue specimen, and the nodes on the opposite side are considered fixed for all degrees of

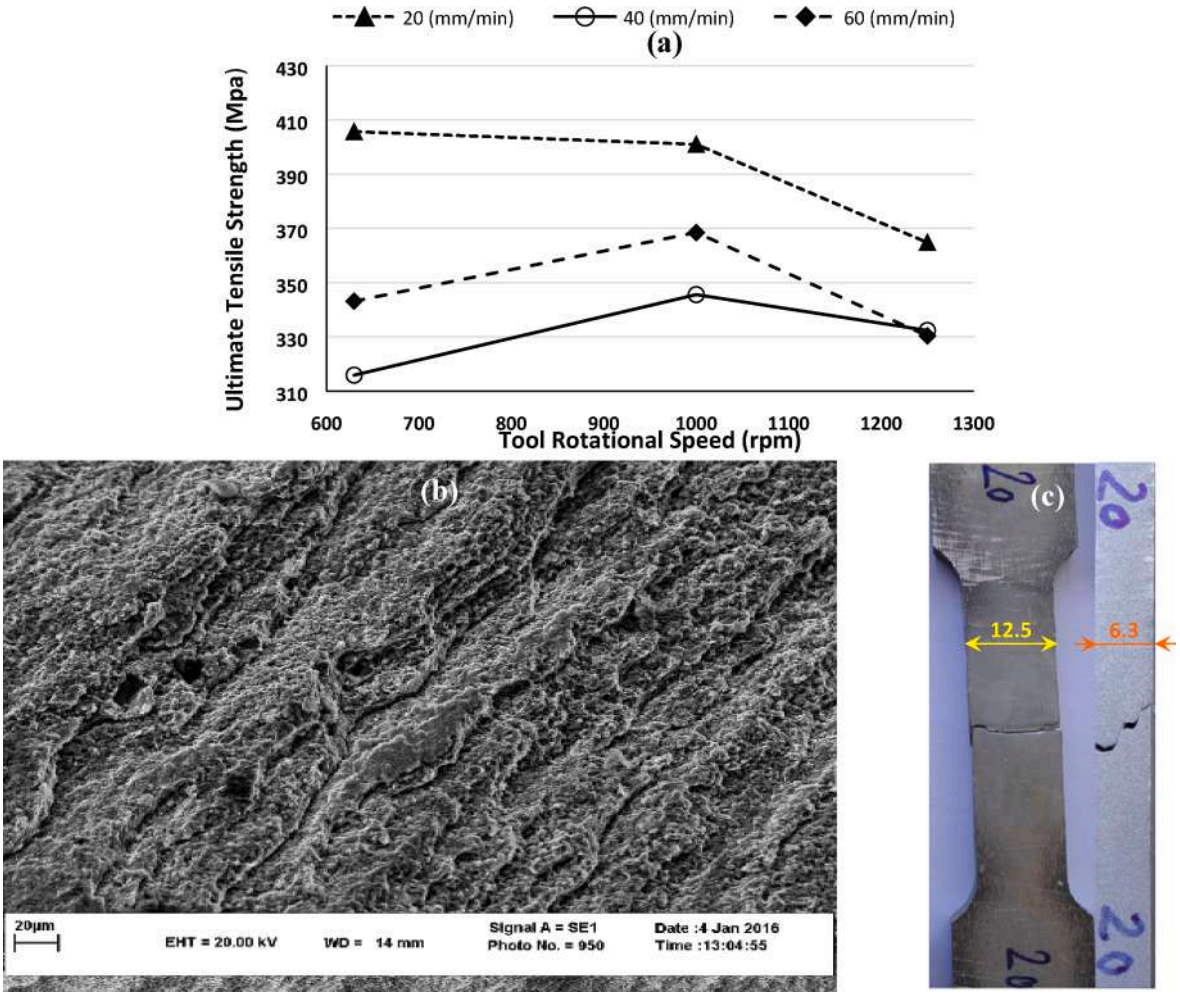

Fig. 11. Simple pin tool; **(a)** UTS in terms of tool rotational speed and welding speed, **(b)** Sample SEM photos of the fracture surface of the joint welded with a Simple pin at 1000 rpm, 20 mm/min, shoulder diameter 22 mm, and **(c)** Photo of the fracture sample.

freedom.

In order to specify the maximum value of the stress concentration factor, a static loading simulation was first performed and the normal stress distribution on the fatigue sample is shown as probed points in Fig. 10. As can be observed from Fig. 10, the maximum stress in the SZ is 184.71 MPa, and the maximum stress concentration factor was 1.24 in the SZ. In addition, Fig. 10 shows that the stresses created in HAZ and BM are about 10% and 25% lower than the maximum stress created in SZ, respectively.

4. Results and discussion

4.1. Ultimate tensile strength and fractography

The impact of pin geometry on the UTS of welded AA7075-T651 aluminum alloy at different tool rotational speeds and welding speeds is shown in Figs. 11–13 for three simple, threaded, and truncated triangular pyramid pins. The two characteristic fracture locations of tensile specimens are shown in Figs. 11–13. According to different welding zones as shown in Fig. 5, the fracture of two specimens in Figs. 11 and 13 occurred near NZ, while the fracture location of Fig. 12 appeared in the transition zone between TMAZ and HAZ. For most of the tensile and fatigue test samples, it happened in the above-mentioned zones, which is also mentioned in Refs [5,33]. In general, with the increase of tool rotational speeds up to 1000 rpm, high tensile strength increases, but after this threshold, the UTS decreases. These observations are due to the impact of frictional heat on the softening of AA7075-T651 aluminum alloy, which causes better mixing of materials inside the joint and better welding. Defect formation in the SZ and SZ size also affect the UTS; For example, large root cavities and incomplete mixing lead to the use of edged pins and reduced SZ size (formed at low tool rotational speed or high welding speed) reduces strength [34,35]. Among the selected pin profiles, the threaded pin joints provide high strength due to the small defect in the SZ. Despite the relationship between SZ size and UTS, the outcomes show that the bond strength decreases

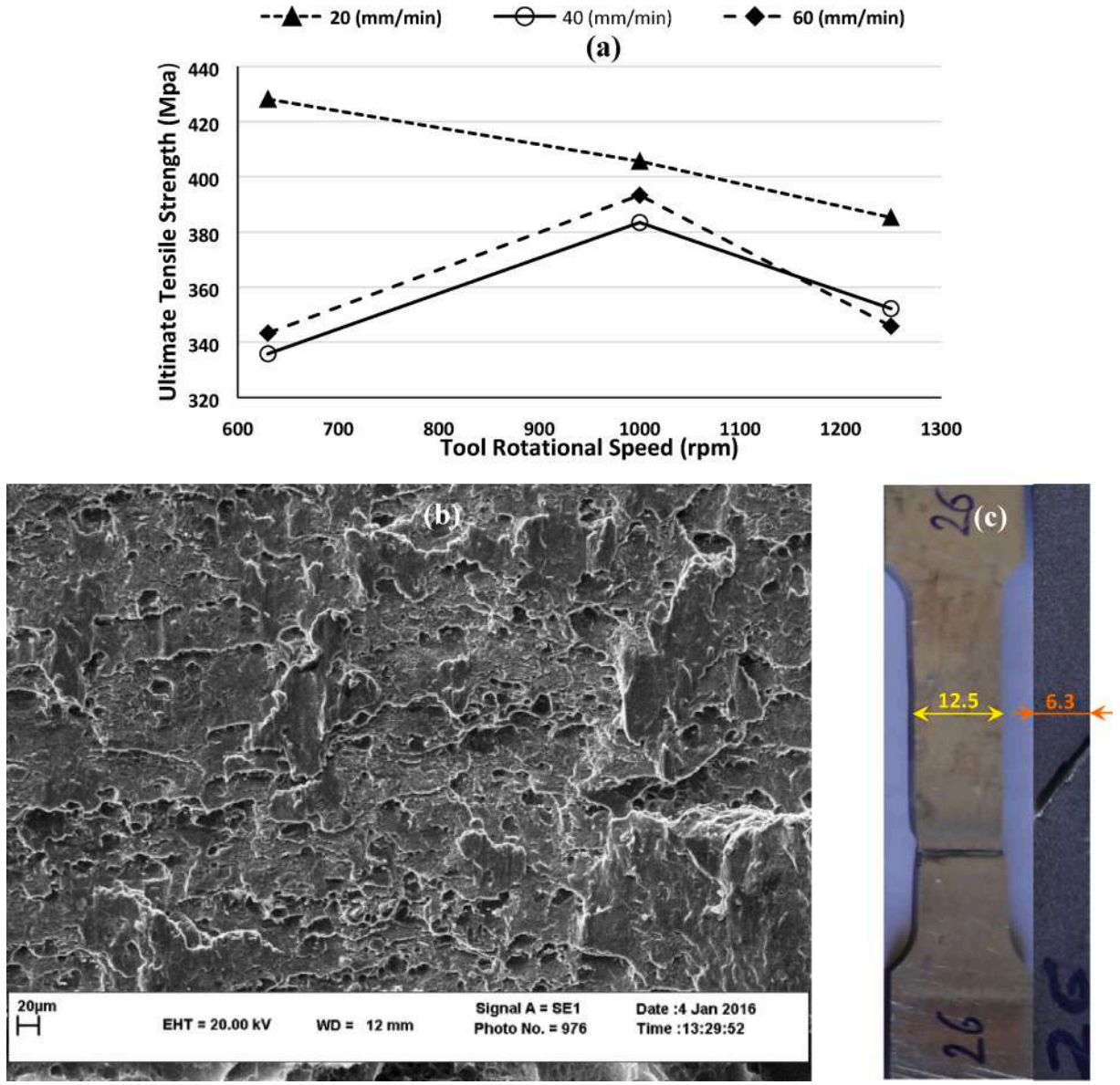

Fig. 12. Threaded pin tool; **(a)** UTS in terms of tool rotational speed and welding speed, **(b)** Sample SEM photo of the fracture surface of the joint welded with a threaded pin at 1000 rpm, 20 mm/min, shoulder diameter 22 mm, and **(c)** Photo of the fracture sample.

remarkably at a tool rotational speed of 1250 rpm.

To find out the effect of pin geometry, SEM photos of the fracture surface of the tested samples under tension were prepared (Figs. 11–13). The SEM photos of the fracture surface of the samples show that the fracture surface of the sample that is welded with the threaded pin is close to the fracture surface of the BM and the relatively high strength of this sample compared to other samples confirms. It was also found that the main reason for the decrease in strength of this sample compared to the BM is internal defects (small holes, cracks, and separated layers). Also, the SEM images of the truncated triangular pyramid pin sample are more prone to break under lower loads than the threaded pin type, which have more internal defects [36].

4.2. Charpy toughness evaluation

An experiment to specify the materials behavior during high loading is impact resistance, which is the amount of energy absorbed in breaking the sample by an impact such as the Charpy experiment according to the ASTM E23-12c standard [37] and Ref [38]. Due to the limitation of materials, a small size sample of Charpy toughness tests with dimensions of 5 × 5 mm was prepared on the FSW joint. The ASTM standard for Notched Bar Impact Testing of Metallic Materials (E23 − 12c) [37] permits the application of sub-size samples

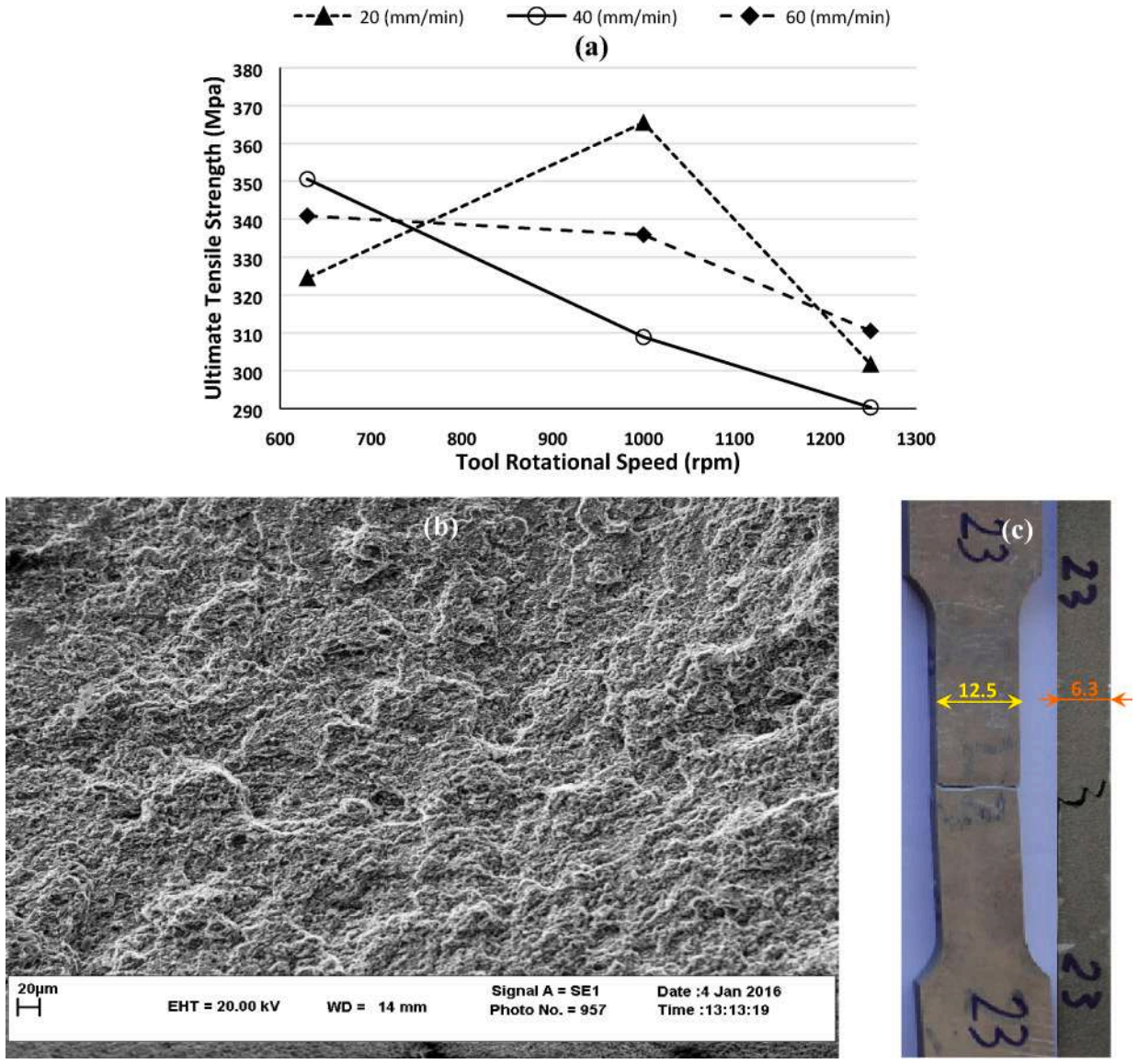

Fig. 13. Truncated triangular pyramid pin tool; **(a)** UTS in terms of tool rotational speed and welding speed, **(b)** Sample SEM photo of the fracture surface of the joint welded with a truncated triangular pyramid pin at (rpm) 1000, (mm/min) 20, (shoulder diameter in mm) 22, and **(c)** Photo of the fracture sample.

Table 4
Comparison of the impact energy results of the joints by the FSW and the BM.

Sample	Base	Simple Pin (SP)	Threaded Pin (TP)	Truncated Triangular Pyramid Pin (TTPP)
Min. Impact Energy (J)	8.8	5.9	6.3	5.1
Max. Impact Energy (J)	10.4	7.5	7.7	6.5

if the amount of material accessible does not allow the manufacture of standard impact experiment specimens. It has been estimated that these sub-sizes cause an error of <0.1 J [39].

To determine and compare the Charpy toughness, impact tests were performed for the BM and the resulting welding joints of three simple, threaded, and truncated triangular pyramid pins at a tool rotational speed of 1000 rpm and a welding speed of 20 mm/min (Table 4). Charpy standard samples were first prepared from the FSW joint and the experiments were done at room temperature. The maximum Charpy energy of V-notch for threaded pin is as follows: maximum Charpy energy = 7.7 J, minimum Charpy energy = 6.3 J.

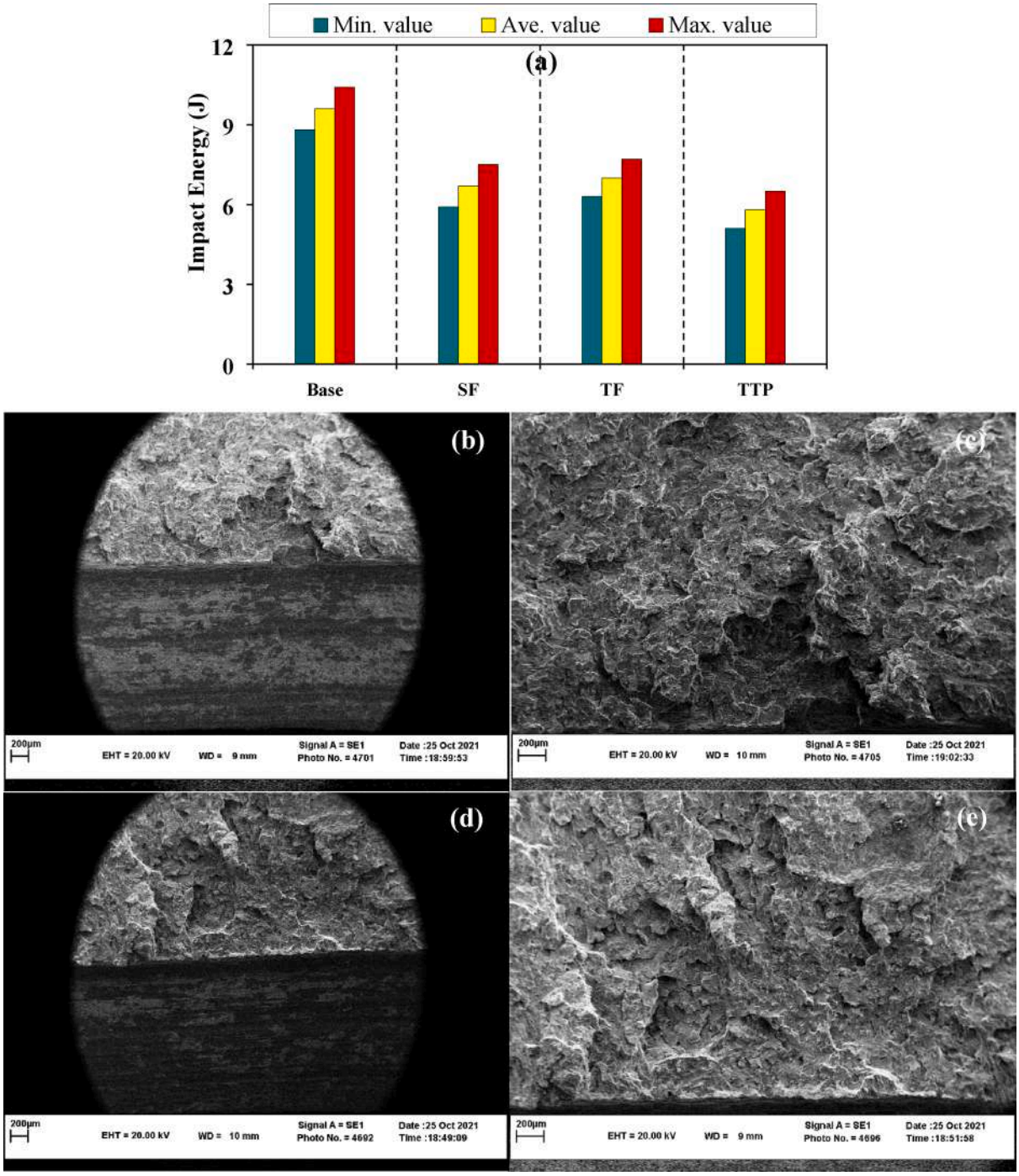

Fig. 14. Charpy experiment results; (a) Determined V-notch Charpy energy, (b), and (c) Charpy sample fracture surface with 65X and 110X magnification with threaded pin, (d), and (e) Charpy sample fracture surface with 65X and 110X magnification in BM.

The results of the Charpy toughness test of the BM and simple, threaded, and truncated triangular pyramid pins show that the maximum impact energy of the welding joints is 72%, 74%, and 63% of the maximum energy of the BM, respectively and for welding joints with a threaded pin is an acceptable amount. In general, the threaded pin specimens are fractured along planes inclined at ≈90° to the cleavage plane, giving a nearly brittle appearance (Fig. 14). The brittle shape resulting from the impact experiment of this material at ambient temperature is alike to the experiment done in Ref [40].

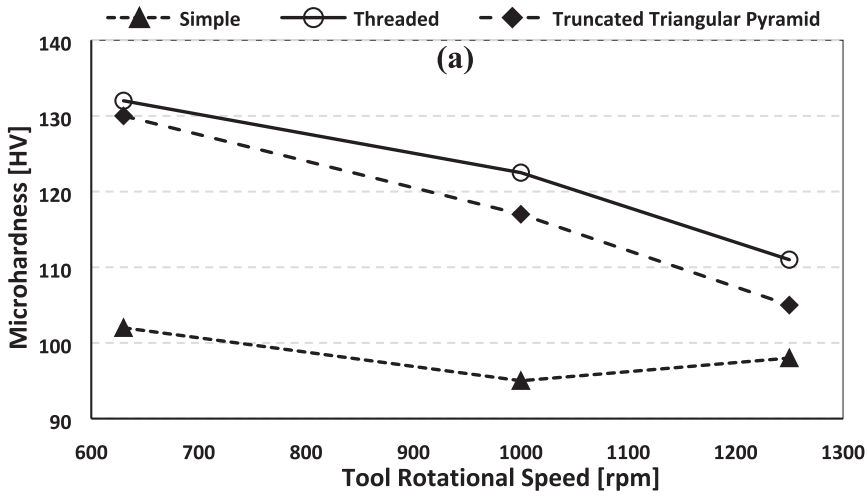

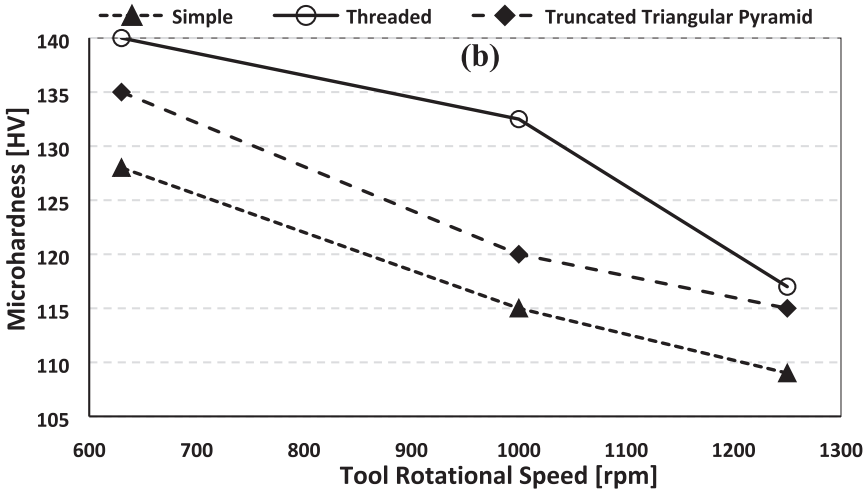

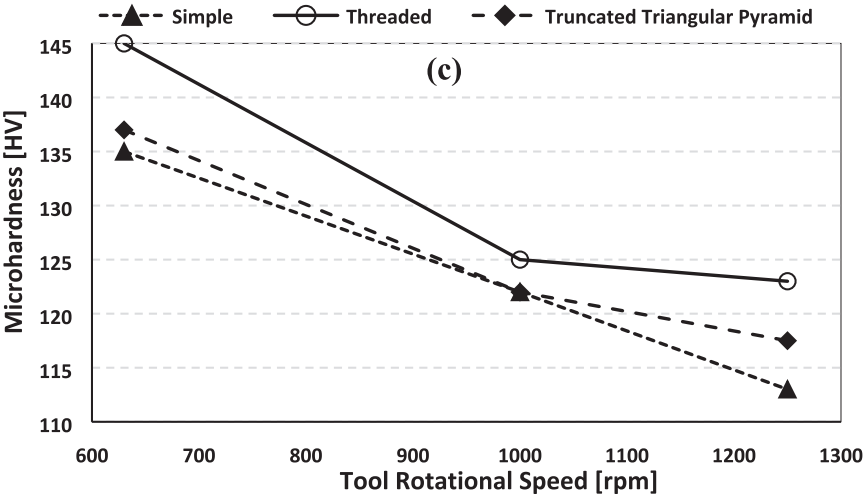

(caption on next page)

Fig. 15. The impact of tool pin geometry on hardness with a shoulder diameter of 22 mm at different tool rotational and welding speeds; **(a)** 20 mm/min, **(b)** 40 mm/min, and **(c)** 60 mm/min.

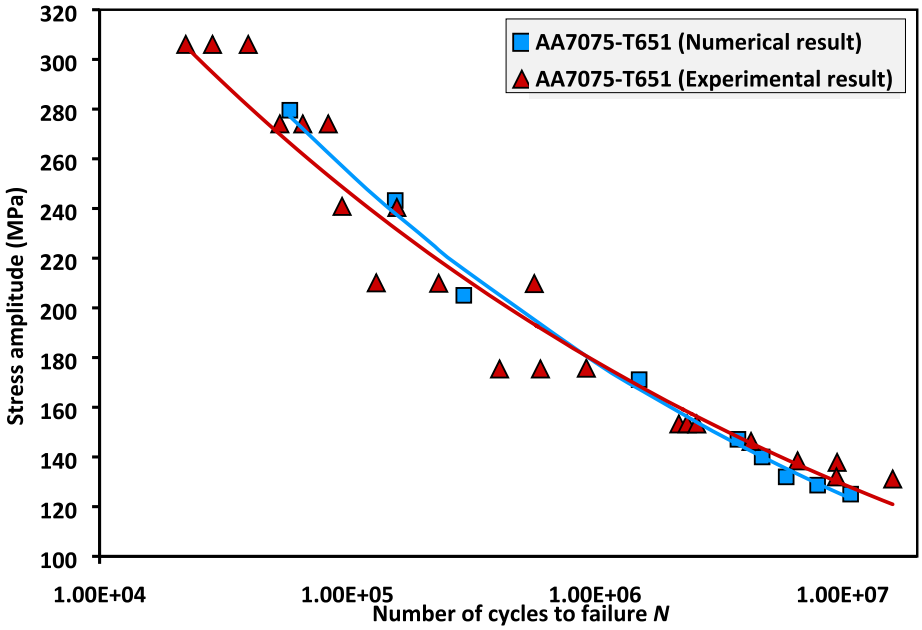

Fig. 16. S-N curves of experimental and numerical results of the AA7075-T651 alloy.

Table 5
The mechanical properties of BM, SP, TP, and TTPP.

Symbol	Ultimate strength (MPa)	Yield strength (MPa)	Modulus of elasticity (GPa)	Poisson's ratio (-)
BM	570	527	71.7	0.33
SP	401	288.5	71.1	0.32
TP	405.6	292.3	71.4	0.32
TTPP	365.5	286.7	70.8	0.31

4.3. Hardness determination

The impact of pin geometry on the hardness of AA7075-T651 aluminum alloy welded by the FSW method was investigated in Fig. 15. The hardness test was obtained in three close rows in before research [34,35]. But in the present manuscript with study comparison of Ref [41] as highlighted in Fig. 6, the middle hardness measurement results in SZ are drawn in the diagrams of Fig. 15. It is interesting to note that the process of hardness changes is distinct from UTS. In truth, the welded material with the highest UTS is softer than the material with the lowest UTS, and vice versa. Under tensile loading, internal defects, voids, and process inclusions play an important role in the mechanical reply, while under compressive loading (such as hardness amount), the impact of material properties becomes more significant. These welds containing more defects (eg, those prepared by truncated triangular pyramid pins) are more sensitive under tensile loading, and failure occurs more rapidly at lower loading levels. Nonetheless, under local compressive loading, the impact of defects decreases while changes in material properties become more beneficial. Insomuch all welds have a lower hardness than the BM, material softening occurred during FSW. This softening appears more at a high tool rotational speed, which indicates the effect of melting and crushing in changing the structure of AA7075-T651 aluminum alloy, which is also mentioned in Ref [5].

4.4. S-N curves

Fig. 16 shows the experimental results and numerical simulation of S-N curves of AA7075-T651 alloy with a stress ratio $R = -1$ in the span of 10^4-10^7 cycles. For FEM calculation, the mechanical properties listed in Tables 2 and 5 have been used, and the properties in Table 5 are in good agreement with the Ref [42]. As the graph shows, a good compromise between the experimental and numerical results of the AA7075-T651 alloy appeared in Fig. 16. The fatigue strength of AA7075-T651 alloy is about 129, 179, and 247 MPa for fatigue life of 10^5, 10^6, and 10^7 cycles, respectively. On the other hand, the outcomes of the numerical simulation exhibited a passable

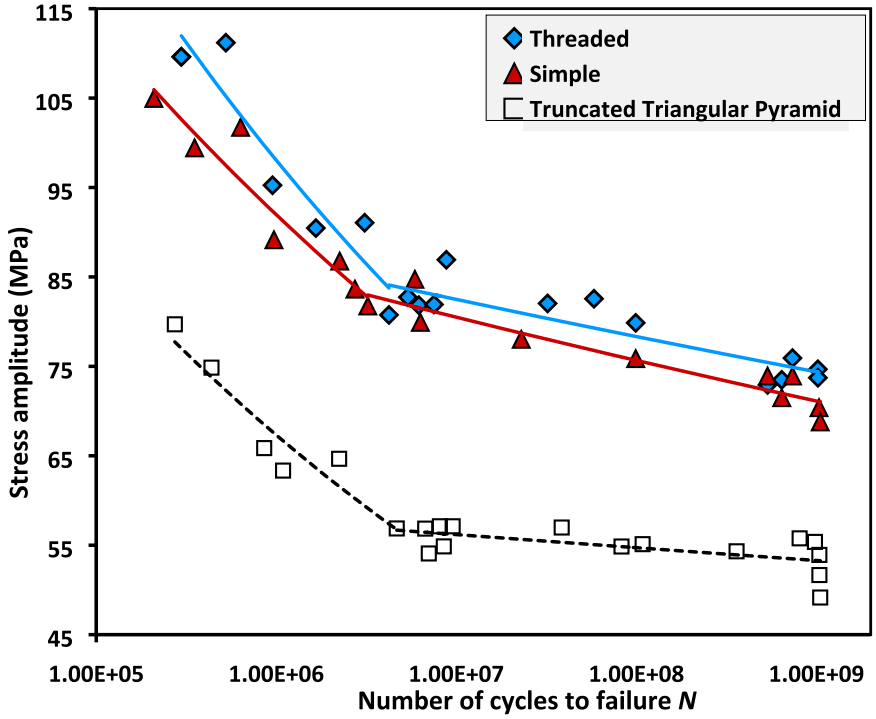

Fig. 17. S-N curves of FSW welding joints of three-pin geometries.

compromise with the experimental outcomes of fatigue, that the error value of the validation of the fatigue life of 10^5, 10^6, and 10^7 cycles was equal to about 3.2%, 0.2%, and −3.4%, respectively.

In Figs. 11–13, nine tensile strength states are drawn for each tool, but due to the time-consuming issue of fatigue, only one optimal state is drawn for each tool in Fig. 17. To simulate and compare the results, the specifications of three simple, threaded, truncated triangular pyramid pins, a tool rotational speed of 1000 rpm, and a welding speed of 20 mm/min were selected. Fig. 17 shows the S-N results of finite element simulation of FSW joints with three simple, threaded, and truncated triangular pyramid pins with stress ratio $R = -1$ in the range of 10^4–10^9 cycles. According to Figs. 16 and 17, it can be seen that the fatigue strength of the FSW joints is remarkably reduced compared to the BM.

As shown in Figs. 11–13, the values of tensile strength for threaded, simple, and truncated triangular pyramid pins was 405.6, 401, and 365.5 MPa, respectively. Also, in Fig. 17, the highest and lowest fatigue strength is related to threaded and truncated triangular pyramid pins, respectively, which is in agreement with the tensile strength diagrams in Figs. 11–13. In 1860 s, Wöhler found for the first time that the relationship between fatigue strength and tensile strength is simply linear. Researchers have developed a well-developed relationship between fatigue strength and tensile strength for many high-strength engineering metallic materials such as steel, copper, and aluminum alloys [43].

During the fatigue life of 10^7 cycles, the fatigue strength is about 83, 81, and 56 MPa for FSW joints of the simple, threaded, and truncated triangular pyramid pins, which constitute 63%, 64%, and 43% of the BM (129 MPa), respectively. In addition, as can be observed from Fig. 17, the fatigue life of the threaded pin shows about 2.4% and 32.5% improvement, respectively, compared to simple and truncated triangular pyramid pins for 10^7. In general, it has been specified that the fatigue life of FSW specimens is always lower than that of BM [44], but FSW joints have better fatigue strength than traditional fusion welds because successful FSW welds do not have inherent or internal defects that the presence of these defects tend to initiate fatigue cracks.

5. Conclusion

In this study, the simulation of fatigue life by FEA in high-strength alloy AA7075-T6 was discussed. In addition, the relationship between the simple, threaded, and truncated triangular pyramid pins as an effective input parameter on the fatigue life of the BM and welded joints was investigated by FEA. Also, the impact of welding parameters such as tool rotational speed, welding speed, shoulder radius, and tool geometry on welding quality including strength, toughness, hardness, and fractography was investigated. The following results were obtained:

(1) The results of the impact of pin geometry on the UTS of AA7075-T651 aluminum alloy welded at different tool rotational speeds and welding speed showed high UTS increases by increasing tool rotational speeds up to 1000 rpm, but after this threshold, the UTS reduces.
(2) The highest UTS (428 MPa; it is about 75% of AA7075-T651 aluminum alloy) was obtained for the geometry of the threaded pin in the transverse direction, and the lowest UTS of the welds was determined for the truncated triangular pyramid pin.
(3) The results of the Charpy toughness test of the BM and three simple, threaded, and truncated triangular pyramid pins showed that the maximum impact energy of welding joints is 72%, 74%, and 63% of the maximum energy of the BM, respectively, and that for welding joints with the threaded pin is an acceptable amount.
(4) The results of the impact of pin geometry on the hardness of the welded AA7075-T651 aluminum alloy showed that the welded material with the highest UTS is softer than the material with the lowest UTS. Most of the hardness was obtained at the low tool rotational speed and high welding speed for all three pins, and the maximum hardness value related to the threaded pin was obtained with a value of 85% of the BM.
(5) Numerical simulation outcomes were in passable compromise with the fatigue experimental outcomes for the BM, and the error value of the validation result for $\sigma_{max} = 0.5\sigma_y$ for the stress ratio $R = -1$ was equal to 0.4%. In addition, the outcomes of the FEA showed that the fatigue strength for FSW joints of the simple, threaded, and truncated triangular pyramid pins in the SZ in the fatigue life of 10^7 cycles was 63%, 64%, and 43% of the BM, respectively.

Declaration of Competing Interest

The authors declare that they have no known competing financial interests or personal relationships that could have appeared to influence the work reported in this paper.

Data availability

Data will be made available on request.

References

[1] C. Deng, H. Wang, B. Gong, X. Li, Z. Lei, Effects of microstructural heterogeneity on very high cycle fatigue properties of 7050–T7451 aluminum alloy friction stir butt welds, Int. J. Fatigue 83 (2016) 100–108.
[2] R.K.R. Singh, R. Prasad, S. Pandey, S.K. Sharma, Effect of cooling environment and welding speed on fatigue properties of friction stir welded Al-Mg-Cr alloy, Int. J. Fatigue 127 (2019) 551–563.
[3] D.M. Neto, P. Neto, Numerical modeling of friction stir welding process: a literature review, Int. J. Adv. Manuf. Technol. 65 (2013) 115–126.
[4] A.R. Shahani, A. Farrahi, Experimental investigation and numerical modeling of the fatigue crack growth in friction stir spot welding of lap-shear specimen, Int. J. Fatigue 125 (2019) 520–529.
[5] F. Zhang, X. Su, Z. Chen, Z. Nie, Effect of welding parameters on microstructure and mechanical properties of friction stir welded joints of a super high strength Al–Zn–Mg–Cu aluminum alloy, Mater. Des. 67 (2015) 483–491.
[6] P. Moreira, T. Santos, S.M.O. Tavares, V. Richter-Trummer, P. Vilaça, P. De Castro, Mechanical and metallurgical characterization of friction stir welding joints of AA6061-T6 with AA6082-T6, Mater. Des. 30 (2009) 180–187.
[7] A.A.M. Da Silva, E. Arruti, G. Janeiro, E. Aldanondo, P. Alvarez, A. Echeverria, Material flow and mechanical behaviour of dissimilar AA2024-T3 and AA7075-T6 aluminium alloys friction stir welds, Mater. Des. 32 (2011) 2021–2027.
[8] C.W. Tan, Z.G. Jiang, L.Q. Li, Y.B. Chen, X.Y. Chen, Microstructural evolution and mechanical properties of dissimilar Al–Cu joints produced by friction stir welding, Mater. Des. 51 (2013) 466–473.
[9] C.B. Fuller, M.W. Mahoney, M. Calabrese, L. Micona, Evolution of microstructure and mechanical properties in naturally aged 7050 and 7075 Al friction stir welds, Mater. Sci. Eng. A 527 (2010) 2233–2240.
[10] K. Krasnowski, C. Hamilton, S. Dymek, Influence of the tool shape and weld configuration on microstructure and mechanical properties of the Al 6082 alloy FSW joints, Arch. Civ. Mech. Eng. 15 (2015) 133–141.
[11] D.M. Rodrigues, A. Loureiro, C. Leitao, R.M. Leal, B.M. Chaparro, P. Vilaça, Influence of friction stir welding parameters on the microstructural and mechanical properties of AA 6016–T4 thin welds, Mater. Des. 30 (2009) 1913–1921.
[12] J. Lukács, Á. Meilinger, D. Pósalaky, High cycle fatigue and fatigue crack propagation design curves for 5754–H22 and 6082–T6 aluminium alloys and their friction stir welded joints, Weld. World. 62 (2018) 737–749, https://doi.org/10.1007/s40194-018-0599-1.
[13] S.J. Maddox, Review of fatigue assessment procedures for welded aluminium structures, Int. J. Fatigue 25 (2003) 1359–1378, https://doi.org/10.1016/S0142-1123(03)00063-X.
[14] C. Sharma, D.K. Dwivedi, P. Kumar, Fatigue behavior of friction stir weld joints of Al–Zn–Mg alloy AA7039 developed using base metal in different temper condition, Mater. Des. 64 (2014) 334–344.
[15] K. Sillapasa, S. Surapunt, Y. Miyashita, Y. Mutoh, N. Seo, Tensile and fatigue behavior of SZ, HAZ and BM in friction stir welded joint of rolled 6N01 aluminum alloy plate, Int. J. Fatigue 63 (2014) 162–170.
[16] X. Liu, L. Zhang, L. Wang, S. Wu, H. Fang, Fatigue behavior and life prediction of A7N01 aluminium alloy welded joint, Trans. Nonferrous Met. Soc. China 22 (2012) 2930–2936.
[17] P. Cavaliere, A. De Santis, F. Panella, A. Squillace, Thermoelasticity and CCD analysis of crack propagation in AA6082 friction stir welded joints, Int. J. Fatigue 31 (2009) 385–392.
[18] Q.Y. Wang, N. Kawagoishi, Q. Chen, Fatigue and fracture behaviour of structural Al-alloys up to very long life regimes, Int. J. Fatigue 28 (2006) 1572–1576.
[19] C. He, Y. Liu, J. Dong, Q. Wang, D. Wagner, C. Bathias, Fatigue crack initiation behaviors throughout friction stir welded joints in AA7075-T6 in ultrasonic fatigue, Int. J. Fatigue 81 (2015) 171–178.
[20] ASTM E1251-17a, Standard Test Method for Analysis of Aluminum and Aluminum Alloys by Spark Atomic Emission Spectrometry, ASTM International, West Conshohocken, PA, 2017. https://doi.org/10.1520/E1251-17A.
[21] A.S.M. Handbook, formerly Tenth Edition, Metals Handbook, vol. 2, Prop. Sel. Nonferrous Alloy. Spec. Purp. Mater. (1990).
[22] ASTM E8 / E8M - 16ae1, Standard Test Methods for Tension Testing of Metallic Materials, ASTM International, West Conshohocken, PA, 2016. https://doi.org/10.1520/E0008_E0008M-16AE01.
[23] K. Aliakbari, K. Farhangdoost, Plastic deformation influence on material properties of autofrettaged tubes used in diesel engines injection system, J. Press. Vessel Technol. Trans. ASME. 136 (2014), https://doi.org/10.1115/1.4026452.

[24] K. Aliakbari, The investigation of modelling material behavior in autofrettaged tubes made from aluminium alloys, Int. J. Eng. 27 (2014) 803–810.
[25] H.E. Boyer, Atlas of Fatigue Curves, ASM International, 1985.
[26] ASTM: E384-11e1, Standard Test Method for Knoop and Vickers Hardness of Materials, ASTM International, West Conshohocken, Pennsylvania, 2011.
[27] J.E. Shigley, Mechanical Engineering Design, McGraw-Hill Companies, 1972.
[28] ASTM: E466 − 15, Standard Practice for Conducting Force Controlled Constant Amplitude Axial Fatigue Tests of Metallic Materials, ASTM International, West Conshohocken, PA, 2015. https://doi.org/10.1520/E0466-15.
[29] K. Langari, Jafar, Farhad Kolahan, Aliakbari, Effect of tool speed on axial force, mechanical properties and weld morphology of friction stir welded joints of a7075–T651, Int. J. Eng. 29 (2016) 403–410, https://doi.org/10.5829/idosi.ije.2016.29.03c.15.
[30] S.-W. Kang, Y.-M. Park, B.-S. Jang, Y.-C. Jeon, S.-M. Kim, Study on fatigue experiment for transverse butt weldsunder 2G and 3G weld positions, Int. J. Nav. Archit. Ocean Eng. 7 (2015) 833–847.
[31] J. Franks, G. Wheatley, P. Zamani, R.M. Nejad, W. Macek, R. Branco, F. Samadi, Fatigue life improvement using low transformation temperature weld material with measurement of residual stress, Int. J. Fatigue 164 (2022), 107137.
[32] K. Aliakbari, S. Kamel Abbasnia, R. Masoudi Nejad, M. Manoochehri, Analysis of stress intensity factors in railway wheel under the influence of stress field due to heat treatment and press-fitting process, Eng. Fail. Anal. (2021) 105736, https://doi.org/10.1016/j.engfailanal.2021.105736.
[33] S.M. Chowdhury, D.L. Chen, S.D. Bhole, X. Cao, Tensile properties of a friction stir welded magnesium alloy: Effect of pin tool thread orientation and weld pitch, Mater. Sci. Eng. A 527 (2010) 6064–6075.
[34] J. Langari, F. Kolahan, The effect of friction stir welding parameters on the microstructure, defects, and mechanical properties of AA7075-T651 aluminium alloy joints, Sci. Iran. Trans. B, Mech. Eng. 26 (2019) 2418–2430.
[35] J. Langari, Numerical and experimental analysis and multi-objective optimization of qualitative characteristics of friction stir welding in 7075 aluminum alloy, Ferdowsi University of Mashhad (in Persian), 2020. Ph.D. Thesis.
[36] H.A. Derazkola, H.J. Aval, M. Elyasi, Analysis of process parameters effects on dissimilar friction stir welding of AA1100 and A441 AISI steel, Sci. Technol. Weld. Join. 20 (2015) 553–562, https://doi.org/10.1179/1362171815Y.0000000038.
[37] ASTM: E23 −12c, Standard Test Methods for Notched Bar Impact Testing of Metallic Materials, ASTM International, West Conshohocken, Pennsylvania, 2012. https://doi.org/10.1520/E0023-12C.
[38] K. Aliakbari, R.M. Nejad, S.K.P. Toroq, W. Macek, R. Branco, Assessment of unusual failure in crankshaft of heavy-duty truck engine, Eng. Fail. Anal. (2022) 106085.
[39] N.H. Fahey, Effects of Variables in Charpy Impact Testing., WATERTOWN ARSENAL LABS MA, 1962.
[40] J. Chao, R. Rementeria, M. Aranda, C. Capdevila, J.L. Gonzalez-Carrasco, Comparison of ductile-to-brittle transition behavior in two similar ferritic oxide dispersion strengthened alloys, Materials (Basel). 9 (2016) 637.
[41] H. Aghajani Derazkola, A. Simchi, Experimental and thermomechanical analysis of the effect of tool pin profile on the friction stir welding of poly(methyl methacrylate) sheets, J. Manuf. Process. 34 (2018) 412–423, https://doi.org/10.1016/j.jmapro.2018.06.015.
[42] M.A.L.I. Fakih, J. Tarraf, S. Mustapha, M.S. Harb, H. Wang, G. Ayoub, R. Hamade, Characterization of Lamb waves propagation behavior in friction stir welded joints of dissimilar materials, Struct. Heal. Monit. 2017 (2017).
[43] J.C. Pang, S.X. Li, Z.G. Wang, Z.F. Zhang, Relations between fatigue strength and other mechanical properties of metallic materials, Fatigue Fract. Eng. Mater. Struct. 37 (2014) 958–976.
[44] L. Ceschini, I. Boromei, G. Minak, A. Morri, F. Tarterini, Effect of friction stir welding on microstructure, tensile and fatigue properties of the AA7005/10 vol.% Al2O3p composite, Compos. Sci. Technol. 67 (2007) 605–615.